Spin–orbit effects in the photodissociation of ionized rare gas trimers: Comparison of He_3^+, Ar_3^+, and Xe_3^+

H. Haberland, A. Hofmann, and B. v. Issendorff
Fakultät für Physik, Universität Freiburg, H. Herderstrasse 3, D-79104 Freiburg, Germany

(Received 22 February 1995; accepted 17 May 1995)

The velocities of neutral and charged photofragments of the rare gas trimers He_3^+, Ar_3^+, and Xe_3^+ have been examined in a comprehensive study for photon energies ranging from 1.5 to 6 eV. For this purpose, a novel time-of-flight technique has been applied which allows the simultaneous examination of both neutral and charged fragments. The general fragmentation pattern of all three species was that of a linear trimer with a parallel transition moment and a totally repulsive excited state: In the course of the dissociation, two of the particles gain high velocities in opposite directions, while the third particle (the middle particle of the linear trimer) only obtains a small velocity. The positive charge generally localizes on one of the fast outer particles, as can be expected from the symmetry properties of the excited state. For Ar_3^+ and Xe_3^+, however, also localization of the charge on the slow particle can be observed. This effect strongly depends on the energy of the absorbed photon, and can be quenched by decreasing the vibrational excitation of the trimer. Comparison of the results with new potential energy surface calculations indicate that mainly spin–orbit coupling induced conical intersections are responsible for this charge redistribution phenomenon. © *1995 American Institute of Physics.*

I. INTRODUCTION

The geometric and electronic properties of ionized rare gas trimers have been subject to a vivid discussion in the recent past. This interest was nourished by their possible influence on the efficiency of excimer lasers and, more generally, by their relative simplicity which makes them model systems for the study of structural and charge delocalization effects. Many theoretical and experimental results are available by now. A number of groups has calculated the structure and the absorption properties of the rare gas trimers (Ar_3^+,[1–4] Xe_3^+,[1] He_3^+,[5] and references therein). The influence of vibrational excitations on the photoabsorption and the fragmentation dynamics of Ar_3^+ have been examined by Ikegami, Kondow, and Iwata[6] and Gadea and Durup.[7] A consistent picture emerges from these calculations. All trimers have a linear and at least nearly symmetrical geometry in the electronic ground state. Their main optical transition in the visible is the transition $\Sigma_u \rightarrow \Sigma_g$ ($\Sigma_g \rightarrow \Sigma_u$ for He_3^+).[8] In Xe_3^+ due to the strong spin–orbit coupling some oscillator strength is given to the transition $\Sigma(1/2)_u \rightarrow \Pi(1/2)_g$, which is weak in Ar_3^+ and does not exist in He_3^+. Vibrational excitations, which have big amplitudes already for the zero-point movements due to the floppy nature of the trimer geometry, give rise to transitions which would be forbidden in a perfect $D_{\infty h}$ symmetry. Namely the bending motion gives some strength to the transition $\Sigma_u \rightarrow \Pi_u$, while the antisymmetric stretching makes the transition $\Sigma_u \rightarrow \Sigma_u$ possible. As at the turning point of the asymmetric stretch the positive charge is localized mainly on the two atoms with the shorter distance, this latter transition can be identified with the transition $\Sigma_u \rightarrow \Sigma_g$ of the ionized dimer (the indices u and g have to be exchanged for the description of the He_3^+). Generally, the charge distribution depends on the state symmetry. In the gerade states of the symmetric linear trimer the charge is equally distributed on the outer atoms, and no charge is located on the inner atom. This follows directly from the state symmetry, if in a simple LCAO description the molecular orbitals are formed only out of the atomic valence orbitals. In the ungerade states about 50% of the charge is located on the inner trimer atom, and about 25% on each of the outer atoms.

Several spectroscopical experiments have been performed on ionized rare gas clusters. The photoabsorption cross sections of Ar_n^+ ions have been measured by a number of groups,[9–11] and recently those of Xe_n^+ and He_n^+ clusters were determined in this group.[11,12] The results obtained for the respective trimers in these experiments were in good agreement with the absorption properties calculated for a linear symmetric geometry. In the recent past, another spectroscopical tool has been applied to examine the bound-free transitions of the ionized rare gas clusters, which is the measurement of the kinetic energy release (KER) to the photofragments. Several groups have performed this kind of experiment on the ionized argon trimer. These studies were restricted to the measurement of the kinetic energy either of the charged monomer fragment at laser wavelengths of 532 nm,[13] of 308 nm,[14] and between 460 and 590 nm,[15,16] or of the neutral fragments at 532 nm.[17,18] The results were similar in all cases: For the neutral as well as for the charged monomer fragments, a bimodal velocity distribution was obtained, that is slow particles with velocities lower than 600 m/s and an isotropic angular distribution were detected as well as fast particles with velocities about 1500 m/s and a $\cos^2$ angular distribution with respect to the direction of the laser polarization. It was further observed that the relative intensity of slow ions increases with photon energy in the examined region between 460 and 590 nm. This appearance of slow ions has given rise to quite a lot of discussion. Since in the excited gerade state of the argon trimer no charge is located on the middle particle, one would naively expect that only fast ions can be formed. It was shown by Ikegami *et al.*[6] and Gadea and Durup[7] in molecular dynamics simulations of the

 0021-9606/95/103(9)/3450/13/$6.00

fragmentation process that nonadiabatic transitions between different states, which are made possible by geometrical distortion due to nonsymmetrical vibrational modes, can be responsible for the slow ion formation. Ikegami *et al.* for example predicted a portion of 23% symmetrical dissociation (that is production of a slow ion) for a trimer with an inner energy corresponding to a temperature of 100 K. This result was obtained without inclusion of spin–orbit effects into the calculations.

In this paper, we want to introduce an improved time-of-flight technique for KER measurements, which allows the simultaneous examination of all charged and neutral photofragments, and this even in the case of clusters with a broad isotope distribution. This method has been applied to study the photodissociation dynamics of He_3^+ in the UV, and of Ar_3^+ and Xe_3^+ in a broad wavelength region from the near UV to the low energy limit of the visible spectrum. The paper is organized as follows: We will first describe the experiment and give a brief introduction into the principles of measuring KER with a time-of-flight technique, then present the measured spectra and last discuss these findings in the light of recent potential energy curve calculations.

This report is intended to focus on the rare-gas trimers. Similar measurements performed on bigger rare-gas clusters will be the subject of forthcoming papers.

II. EXPERIMENT

The measurements were done in a tandem time-of-flight mass spectrometer (TOF-MS).[19] This setup of two sequential TOF-MS (a reflectron mass spectrometer followed by a linear TOF-MS) was chosen for the following reason: for measurements of the kinetic energy release with a time-of-flight technique a single linear TOF-MS is sufficient only in cases where the cluster atoms have one dominant stable isotope. Cluster ions of elements with broad isotope distributions (like xenon) produce TOF peaks so broad that peak shifts due to kinetic energy release are not resolvable. Therefore in the case of xenon the first spectrometer was used as a mass preselector, which cuts a small slice (about 10%–20%) out of the broad mass distribution of a given cluster size, and with this reduced cluster packet then the actual experiment was performed in the second spectrometer. In the cases of the almost monoisotopical helium and argon clusters this tandem arrangement is not absolutely necessary, but leads to noise reduction since only one cluster size is extracted into the second spectrometer.

The arrangement is shown schematically in Fig. 1. Two types of nozzles were used to produce the neutral clusters. A conical nozzle (diameter 80 μm, conus angle 30°, conus length 2 mm, stagnation pressure 2.5 bar) was taken for the production of argon or xenon clusters. In the first case, pure argon gas was expanded through the nozzle, while in the second case a mixture of 5% xenon in argon was used. The helium clusters were produced with a coolable nozzle (diameter 5 μm, source temperature 8–20 K, stagnation pressure 50 bar). Details of this source are given in Ref. 20.

The neutral clusters produced in the expansion pass through a 0.7 mm diameter skimmer and subsequently traverse a pulsed electron beam (energy 200 eV). Ionized clusters are extracted out of the neutral beam under an angle of 5° and accelerated into the reflectron TOF-MS.

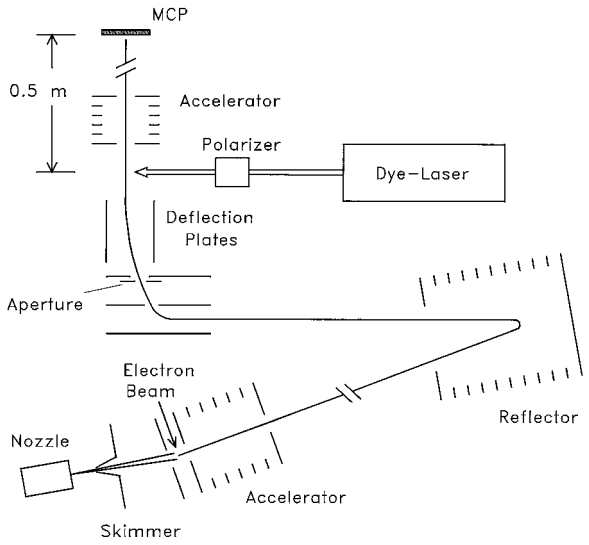

FIG. 1. Schematic diagram of the apparatus. The reflector angle of 2° is highly exaggerated.

The second TOF-MS is located behind the reflector in the spatial focus of the first TOF-MS. In principle it is a linear Wiley–McLaren-type TOF-MS with an axis perpendicular to the beam axis of the first mass spectrometer. Preselected cluster ions are extracted into this second spectrometer by a high-voltage pulse applied to the first stage of the two stage accelerator. Behind the accelerator the cluster beam is bent into a fully perpendicular direction by applying a high-voltage pulse to a pair of deflection plates. A pulsed field is used here in order to bend the beam without spoiling the TOF resolution in the flight direction. At the end of the accelerator the cluster ions pass through a 3 mm slit aperture. This slit serves as a mass selector: In the focus point of a TOF-MS a packet of clusters having one isotope only will have a length Δx determined by the resolution of the apparatus and the total flight length ($\Delta x \approx 1.5$ mm here). If, however, the cluster atoms have a number of isotopes, the packet length will be determined mainly by the broadness of the mass distribution ($\Delta x \approx 25$ mm in the case of Xe_3^+). If such a long packet is pulsed into the accelerator, only a small slice of it will pass the aperture. Provided that the spectrometer focus point spatially coincidences with the aperture position, this slice will have a narrow mass distribution. The mass resolution of this ''mechanical chopper'' depends on the resolution of the first mass spectrometer and on the aperture width. With the 3 mm aperture chosen here a resolution of about $m/\Delta m = 300$ is obtained, which provides sufficient TOF resolution in the second spectrometer together with a reasonable intensity.

After passing a drift length of 0.5 m the cluster ions are detected by a special multichannel plate (MCP) detector. In this detector the electrons produced by a single stage MCP are accelerated by about 15 kV onto a plastic scintillator. The light produced here is then led through a lightguide to a photomultiplier in a well shielded housing outside of the

apparatus. This arrangement has the advantage of combining a very high single event pulse height with a very low noise. Even the several strong high-voltage pulses used in the experiment have almost no influence on its signal due to the good shielding of the photomultiplier. The analog signal produced by the detector finally is digitized by a fast transient recorder (100 MHz, 8 bit).

The photofragmentation of the clusters takes place behind the the Wiley–McLaren accelerator and the deflection plates at the beginning of the drift region (cf. Fig. 1), where the ion beam is crossed by a polarized laser pulse of an excimer pumped dye laser (Lambda physics, pulse duration $\approx$10 ns). The center-of-mass velocities of the cluster fragments gained in the dissociation process then lead to a splitting or broadening of the TOF peaks. In order to separate fragments of different masses, an acceleration field is placed behind the laser interaction zone, which is chosen weak enough (potential difference of 10% to 20% of the cluster ion kinetic energy) not to affect the temporal resolution of the TOF setup. Not only charged but also neutral photofragments are detected by the MCP because they have kinetic energies of several hundred volts, stemming from clusters with a kinetic energy of typically 3000 V. With this apparatus it is thus possible to measure the center-of-mass velocity distributions of all fragments (charged and neutral) in one spectrum at the same time. The measured flight times are very precise because scattered light of the laser pulse produces a signal on either the MCP or the photomultiplier of the particle detector. As this yields an exact time zero, no delay times of preamplifiers or trigger lines have to be taken into account. Typically 5000 to 15 000 sweeps have been averaged to obtain one spectrum, which at a laser frequency of 25 Hz results in a measuring time of 4 to 15 min per spectrum.

Cooled argon trimers. The helium cluster source was also used to produce ionized argon clusters with a reduced vibrational excitation. Argon atoms were embedded into neutral helium clusters by simply applying an argon background pressure of about 10^{-4} mbar to the second chamber of the apparatus. In this chamber the helium clusters cover a path of about 50 mm between the skimmer and the ionizing electron beam. After electron impact ionization of these doped helium clusters pure ionized argon clusters as well as such with one, two or more attached helium atoms could be observed. Out of these the cluster Ar_3^+He was selected for a photofragmentation experiment intended to be performed on a ''cooled'' argon trimer.

Generally ionized argon clusters produced by electron impact ionization of neutral argon clusters are vibrationally highly excited due to the large binding energy and bond length differences between neutral and ionized clusters. If, however, an argon cluster is ionized inside a helium cluster, its vibrational energy will be released by evaporation of helium atoms. The amount of released internal energy of course depends on the initial size of the helium cluster, so that no definite value can be given for the vibrational energy of an ionized argon cluster which has lost all of its surrounding helium atoms. For those clusters which after the evaporation end up with one or more helium atoms still attached, at least an upper limit for this internal energy can be given. As the binding energy of a helium atom to an argon trimer will be less than that to a helium trimer, the inner energy of the Ar_3^+He will be less than 30 meV [which is the binding energy of a helium atom to a He_3^+ (Ref. 21)]. This is much less than the energy which can be stored in a pure ionized argon trimer [D_0=210 meV for Ar_3^+ (Ref. 24)]. Assuming that the attached helium atom does not affect the photoabsorption or fragmentation properties of the argon trimer, thus with the species Ar_3^+ and Ar_3^+He, two argon trimers of different ''temperatures'' are available for the photofragmentation experiments.

III. EVALUATION METHOD

The measured TOF spectra have been fitted with model functions, which will be briefly described in this section.

A. Time-of-flight distributions

The model functions result from the transformation of center-of-mass (c.m.) velocity distributions to temporal distributions:

$$\tilde{f}(t)dt = f(v_\parallel)(s/t^2)dt, \tag{1}$$

$$v_\parallel(t) = s/t - v_0. \tag{2}$$

Here v_0 is the original cluster velocity, $v_\parallel$ the projection of the c.m. velocity of the fragments onto the beam direction, and s the flight path length. The distribution $f(v_\parallel)$ of the projected velocities depend on the absolute values of the c.m. velocities as well as on the respective angular distributions. The angular distribution of a fragment is determined by three entities: by the absorption probability, which is proportional to $(\boldsymbol{\mu}\mathbf{E})^2$ ($\boldsymbol{\mu}$ being the transition moment, and $\mathbf{E}$ the electric field vector), by the angle between the fragment velocity and $\boldsymbol{\mu}$, and by the angle between $\mathbf{E}$ and the beam axis. So if for example a dimer with a transition moment parallel to its axis is dissociated by a laser beam polarized parallel to the beam axis, an angular distribution proportional to $\cos^2\theta$ is obtained (θ being the angle between the fragment velocity and the beam axis). A distribution proportional to $\sin^2\theta$ will be obtained if the laser is polarized perpendicular to the beam axis, or if the dimer has a perpendicular transition moment. Isotropic distributions will occur if the ejection direction of the photofragment is not coupled at all to the direction of the transition moment.

For this three ''model'' cases the resulting time-of-flight distributions are easily calculated. Assuming a fixed c.m. velocity v, the following three $f(v_\parallel)$ are obtained for the respective angular distributions ($v_\parallel = v\cos\theta$):

$$f_\parallel(v_\parallel) = \chi_{-v,v}(v_\parallel)\,\frac{3v_\parallel^2}{2v^3} \qquad \tilde{f}_{\text{c.m.}}(\theta) \propto \cos^2\theta, \tag{3}$$

$$f_\perp(v_\parallel) = \chi_{-v,v}(v_\parallel)\,\frac{3}{4v}\left(1-\frac{v_\parallel^2}{v^2}\right) \qquad \tilde{f}_{\text{c.m.}}(\theta) \propto \sin^2\theta, \tag{4}$$

$$f_{\text{iso}}(v_\parallel) = \chi_{-v,v}(v_\parallel)\,\frac{1}{2v} \qquad \tilde{f}_{\text{c.m.}}(\theta) \propto 1. \tag{5}$$

Here χ is the characteristic function

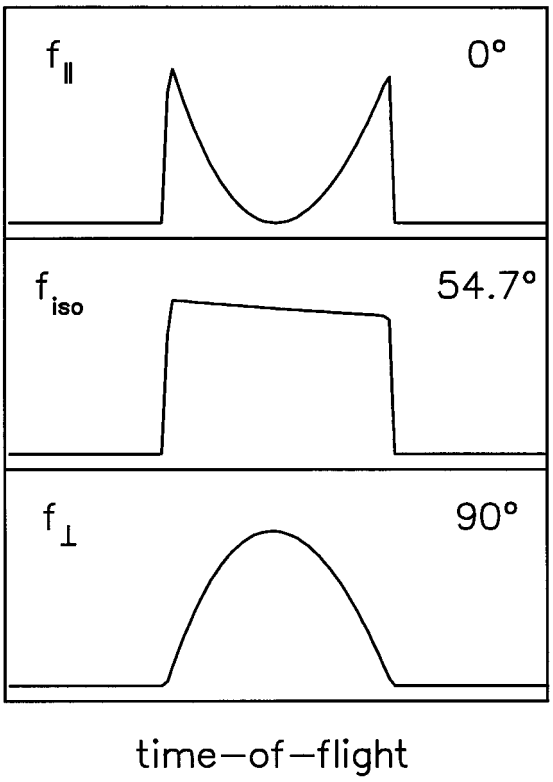

FIG. 2. Time-of-flight distributions which result for three cases of angular distributions of the fragments in the center-of-mass system: $\cos^2$, $\sin^2$, and isotropical distribution with respect to the beam axis. In the case of a dimer with a parallel transition moment these distributions result for the given angles between laser polarization and beam axis.

$$\chi_{a,b}(x)=\begin{cases}1 & x\in[a,b],\\ 0 & x\notin[a,b].\end{cases} \tag{6}$$

The TOF spectra which following (1) and (2) result from these projected velocity distributions are schematically shown in Fig. 2. The $\cos^2$ distribution ($f_\parallel$) obviously leads to a wing structure formed like a parabola, whereas the $\sin^2$ distribution ($f_\perp$) produces a peak like an upside down parabola. The isotropic distribution ($f_{\rm iso}=1/3(f_\parallel+2\ f_\perp)$) produces a rectangular peak form. All peak structures show a weak decline in the direction of the time axis due to the transformation Jacobian $1/t^2$.

This simple distributions are correct only for some special systems. In more general cases, the projected velocity distributions can be described by

$$f(v_\parallel)=\tfrac{3}{2}[(k-\tfrac{1}{3})f_\parallel(v_\parallel)+(1-k)f_{\rm iso}(v_\parallel)], \tag{7}$$

where the parameter k is given by

$$k=\cos^2\gamma\,\cos^2\beta+\frac{\sin^2\gamma\,\sin^2\beta}{2}. \tag{8}$$

Here β is the angle between the fragment c.m. velocity and the transition dipole moment of the molecule, and γ is the angle between the direction of the laser polarization and the beam axis. Note that if either of these has a value of 54.7°, a projected velocity distribution identical to that of an angularly isotropically distributed fragment results.

The above described refers to the time-of-flight spectra of the neutral fragments. For the charged fragments the acceleration after the laser interaction has to be taken into account. Fortunately it turned out that the acceleration does not destroy the mainly linear and slightly quadratic dependence of the flight times on the c.m. velocities, so that by replacing the true flight length and the true initial cluster velocities by calculated values the formulas deduced for the neutral fragments can be used for any charged fragment.

B. Fitting parameters

Because of the floppy nature of the trimers the fragmentation out of a distorted geometry has to be taken into account. In such a situation the middle particle can pick up a quite high velocity, due to which the velocities of the outer particles can differ considerably. In order to use as few fitting parameters as possible, the conversation of energy and momentum have been used to inter-relate the velocities of the three trimer fragments. For the middle particle, an angularly isotropic Boltzmann type velocity distribution has been assumed

$$f(v,\theta)\propto v e^{-v^2/2\sigma^2}. \tag{9}$$

The velocities of the outer particles have then been calculated following:

$$\mathbf{v}_1+\mathbf{v}_2+\mathbf{v}_3=0, \tag{10}$$

$$\frac{m}{2}\,(\mathbf{v}_1^2+\mathbf{v}_2^2+\mathbf{v}_3^2)=E_{\rm kin}. \tag{11}$$

The assumption of a parallel transition moment has been accounted for by defining the direction of the transition moment as

$$\frac{\boldsymbol{\mu}}{|\boldsymbol{\mu}|}=\frac{\mathbf{v}_1-\mathbf{v}_3}{|\mathbf{v}_1-\mathbf{v}_3|}. \tag{12}$$

$\mathbf{v}_1$ and $\mathbf{v}_3$ are the velocities of the outer particles. Due to this equation, the outer particles have equal c.m.-velocity components perpendicular to the transition moment, which is exactly valid for the fragmentation of a symmetrical bend trimer or of a linear asymmetrically stretched trimer, but only approximately in intermediate cases.

For the calculation of the TOF spectra the finite solid angle of the detector has been taken into account via a Monte Carlo routine, and the temporal resolution was included by convoluting the resulting spectra with the measured TOF-peak of the unfragmented cluster.[22] Thus besides the amplitudes of the slow and fast particles and a factor which models the small correction due to the velocity dependent detection probability of the MCP only two main fitting parameters were used, that is the width of the velocity distribution of the middle particle and the overall released kinetic energy.

In this way the total kinetic energy of all three fragments could be extracted from the measured spectra, which is essential for a reliable determination of the binding energies.

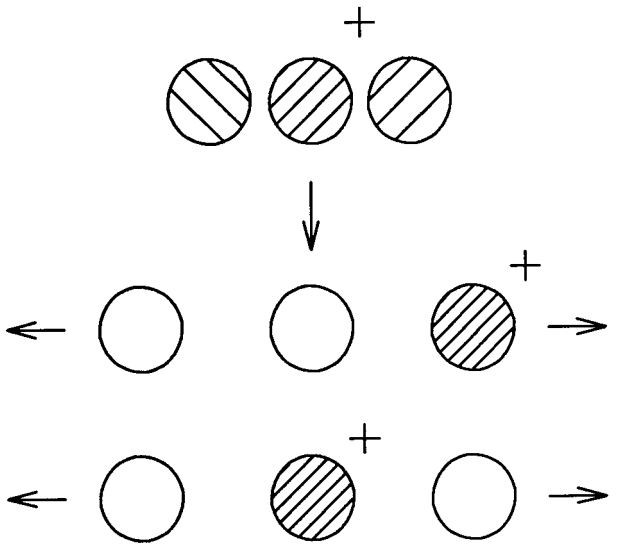

FIG. 3. The two possible channels for the dissociation of a charged linear trimer in a totally repulsive excited state: the positive charge can localize on the middle atom ("symmetric fragmentation") or on one of the outer atoms ("asymmetric fragmentation").

C. Fragmentation symmetry

Additional to the kinetic energy another important feature is obtained from these fits, which is the symmetry of the fragmentation. This will be explained with the help of Fig. 3. The overall fragmentation pattern of a linear trimer is nearly always the same: Because of the fact that the excited states are totally repulsive the outer atoms of the trimer will gain high velocities to either side, while the middle particle will only obtain a very small c.m. velocity. For the localization of the positive charge two possibilities occur: It can either localize on one of the outer atoms, thus leading to the production of one fast and one slow neutral as well as one fast ion, or it can localize on the middle atom, thus leading to the production of two fast neutrals and one slow ion. The two processes will be called asymmetrical and symmetrical fragmentation, respectively. The branching ratio between these processes are determined from the relative intensities of slow and fast particles. Since in every fragmentation two neutral fragments are produced, but only one charged fragment, the calculation of the branching ratio depends on whether the intensities of the neutral monomer or of the charged monomer fragments are evaluated. The amount of symmetrical fragmentation α_{sym} for example is obtained from the respective intensities of slow (I_s) and fast (I_f) particles following:

$$\alpha_{\mathrm{sym}}=\frac{I_s}{I_f+I_s} \qquad \text{charged monomers,} \tag{13}$$

$$\alpha_{\mathrm{sym}}=\frac{I_f-I_s}{I_f+I_s} \qquad \text{neutral monomers.} \tag{14}$$

This evaluation of the relative intensities is most reliable for the spectra recorded at a laser polarization angle of 54.7°, since no angular distributions have to be taken into account here. Evaluating both charged and neutral fragment intensities further reduces the uncertainty of the result, since possible systematic evaluation errors (e.g., an incorrect choice of the exact form of the middle particle velocity distribution) cancel out this way.

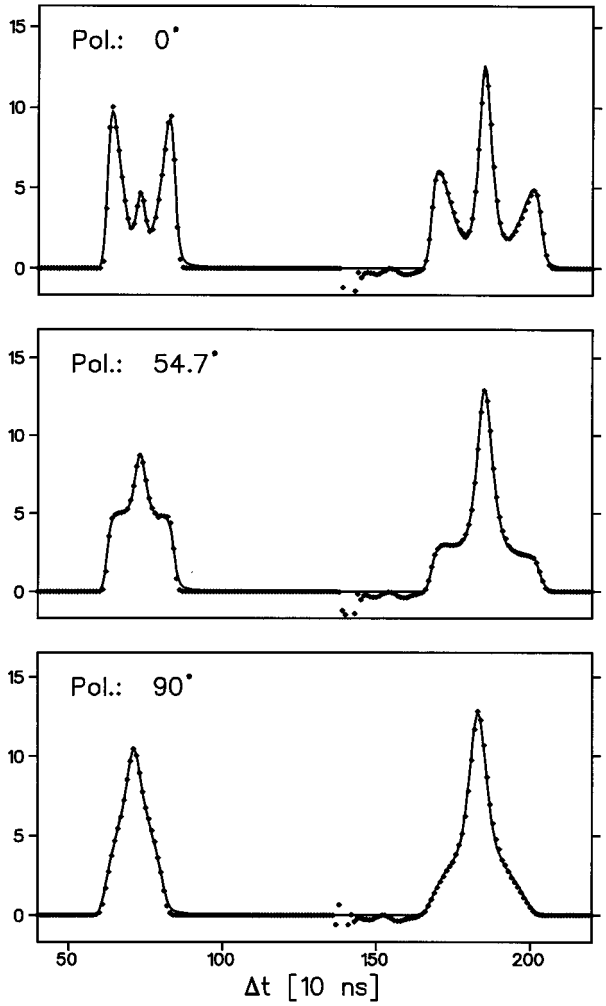

FIG. 4. Fragment TOF spectra of Ar_3^+ at $\lambda=480$ nm, obtained for three different angles between the laser polarization and the beam axis. From left to right first the charged and then the neutral monomer fragment appear. The peak of the unfragmented trimers has been suppressed here. Note the characteristic form of the different distributions (cf. Fig. 2).

D. Example spectra

In Fig. 4, three examples of TOF spectra are shown. These are spectra of the photofragments of Ar_3^+, dissociated at a photon wavelength of 480 nm (2.58 eV) and three different angles between the laser polarization and the beam axis. Only the fragments Ar_1^+ (left) and neutral Ar_1 (right) are visible; charged dimer fragments do not appear in this photon energy region, and the peak of the unfragmented trimers has been suppressed by subtracting a spectra recorded without laser excitation. Both fragments appear with either a high or a low velocity, which can be seen best in spectrum (a). The TOF distributions of the fast particles indicate that they have a $\cos^2$-like angular distribution with respect to the laser polarization. At the three polarization angles the theoretical distributions calculated for this case are well reproduced (cf.

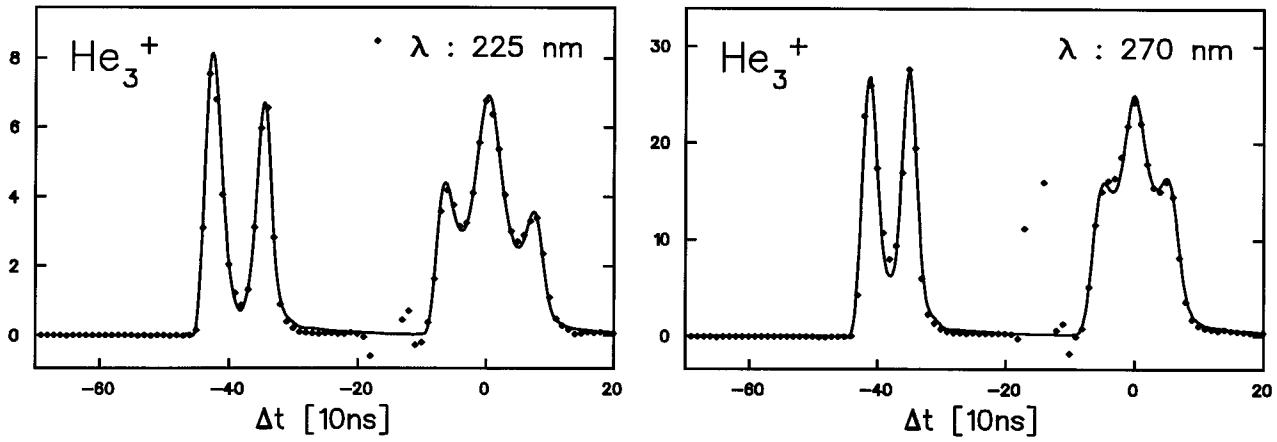

FIG. 5. Fragment TOF spectra of He_3^+ at two different wavelengths, laser polarization parallel to the beam. The fragments He_1^+ and neutral He_1 appear from left to right.

Fig. 2). The slow particles, the peaks of which are added on top of the respective fast particle peaks, seem to have an isotropic angular distribution, as the peak form does not change with the laser polarization angle. Note that the relative intensities of the fast and slow particles are easiest to evaluate at the ''magic'' polarization angle of 54.7°.

At most wavelengths the trimer photofragment spectra have been measured for all of this three polarization angles. In the following, however, only the spectra obtained for parallel polarization are shown, since they convey the most information.

IV. RESULTS

TOF spectra of the photofragments of He_3^+ measured at the wavelengths $\lambda=225$ and 270 nm are shown in Fig. 5 (the lowest absorption band of He_3^+ is centered at about 230 nm[12]). The full lines drawn through the data points reproduce the fitted model functions. Only neutral and charged monomer fragments appear; the peak of the unfragmented trimers has been suppressed here and like in all other spectra by subtracting a spectrum recorded without laser excitation, so that only a noiselike structure can be seen at the position where it would appear. The neutral monomers exhibit again a peak structure, which consists of a central peak of particles which have gained no or only a low center-of-mass velocity during the dissociation, and of a pair of wings, which indicate fast particles ejected in and against the flight direction of the trimers. Obviously for the charged monomers only fast particles appear, while for the neutral fragments an equal amount of fast and slow particles are detected. This pattern does not change with photon energy; the only feature which changes is the wing separation, which indicates that the kinetic energy of the fast particles increases with increasing photon energy, as has to be expected because of the conversation of energy. Evaluation of the total kinetic energy yields a binding energy of the trimer of 2.6 ± 0.15 eV. This large uncertainty is not due to the apparatus resolution, but to a certain ambiguity in the choice of the angular and velocity distribution of the middle particle.

The fragment TOF spectra of the Ar_3^+ fragments are depicted in Fig. 6. Since the argon trimer ion does absorb in a much broader wavelength region, a higher number of spectra have been recorded. Basically, except for the very low photon energies, the spectra are very similar to those of the helium trimer. The main difference is that in the case of the argon trimer also slow charged monomers appear. Another difference is that here at the low photon energies charged dimer fragments are formed as well. The most interesting feature, however, is the wavelength dependence of the slow ion appearance, that is of the fragmentation symmetry. The amount of symmetric fragmentation has been extracted from the different TOF spectra according to (13) and (14), and is shown in Fig. 7 as a function of the photon energy. In the region between 2.1 and 2.7 eV this ratio indeed does increase with photon energy, as observed by Kondow and coworkers.[16] The overall behavior, however, is more complicated than a simple monotonic dependence on the energy. The ratio exhibits a maximum around 3.3 eV, and it also rises again below 2.0 eV. Although spectra have been measured down to photon energies of 1.65 eV, no results are given for energies below 1.9 eV. In this region the distinction between fast and slow particles is somewhat arbitrary, because the distributions of both strongly overlap.

In Fig. 8 the results of the examination of the temperature dependence of this dissociation symmetry are shown. Obviously at all examined wavelengths the Ar_3^+He, which is assumed to be equivalent to an argon trimer with a reduced internal energy, has a stronger preference to asymmetrical fragmentation than the pure, probably strongly vibrationally excited argon trimer. Of course it has to be discussed whether this reduction of the slow ion intensity is caused by the attached helium atom. This seems to be very unlikely, as because of the large difference in the ionization potentials of argon and helium atoms no charge can be transferred to the attached helium atom, i.e., it can be considered as a spectator atom which only interacts with the trimer via its very small polarizability. Moreover, an influence of the He atom would rather increase the slow ion intensity than reduce it, as was observed recently for the case of the photofragmentation of

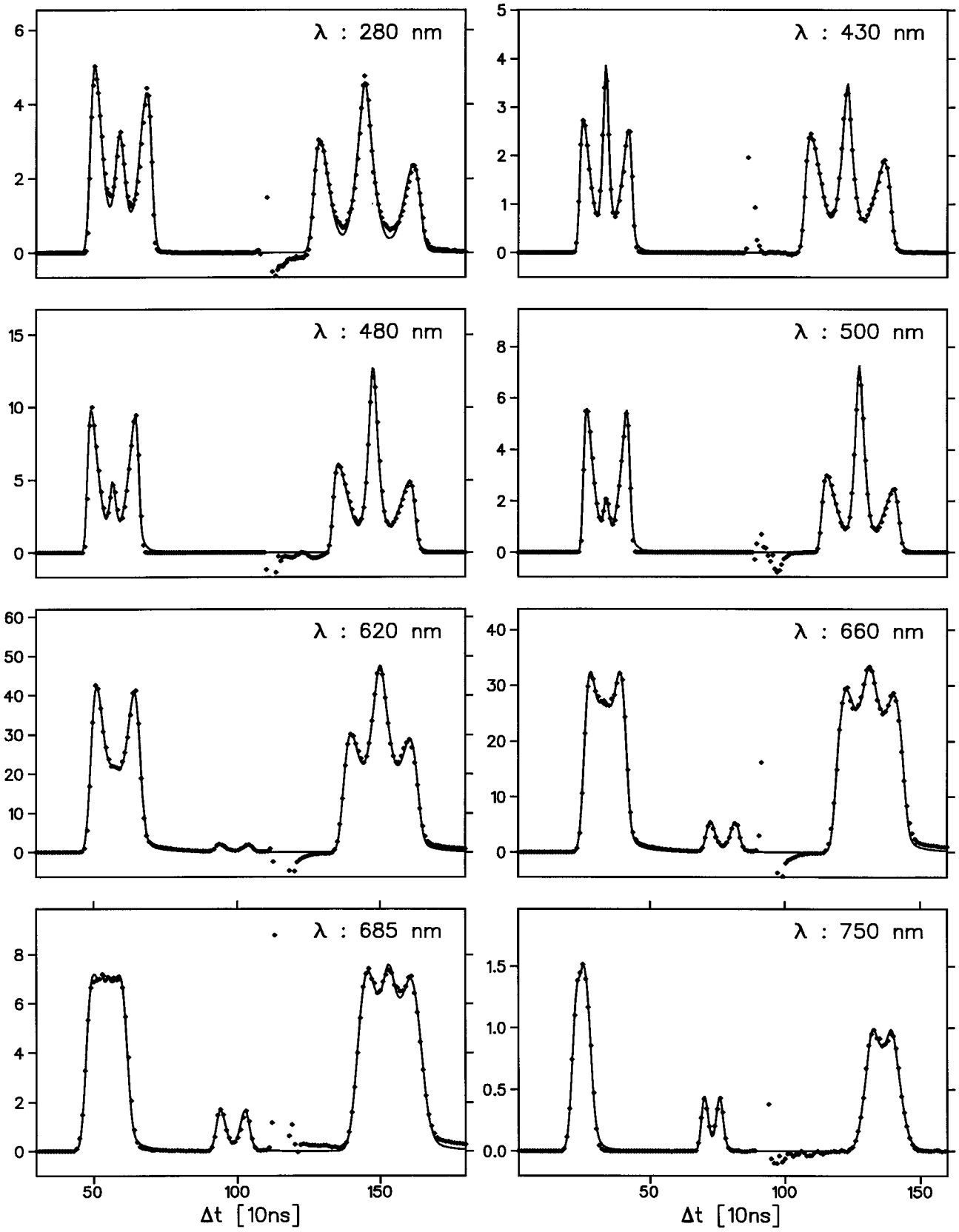

FIG. 6. Fragment TOF spectra of Ar_3^+ at different wavelengths, laser polarization parallel to the beam. The fragments Ar_1^+ and neutral Ar_1 appear from left to right. For the low photon energies additionally Ar_2^+ fragments are visible.

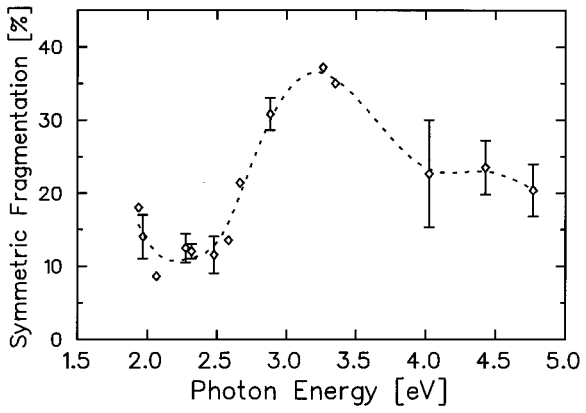

FIG. 7. Amount of symmetric fragmentation of Ar_3^+ as function of the photon energy (cf. Fig. 3).

He_3^+ and He_4^+. He_4^+ consists of a linear charged trimer with a loosely attached helium atom, and here the attached atom indeed strongly increases the abundance of the slow ions.[12]

In Fig. 9, the total kinetic energies of the photofragments are shown as a function of the photon energy. The two lines give the kinetic energy which could be expected for a binding energy of the trimer of 1.54 eV,[23,24] and the two possible states of the argon ion (ΔE_{SO}=0.18 eV). Obviously for the lower photon energies the measured kinetic energies lie well on the upper line, indicating that the ion is formed in the lower $^2P_{3/2}$ state, while for the highest photon energies the ion seems to be formed in the higher $^2P_{1/2}$ state.

Figure 10 shows the fragment TOF spectra of the xenon trimer. At wavelengths longer than 640 nm, the peak pattern is again very similar to that of He_3^+, that is, no slow charged

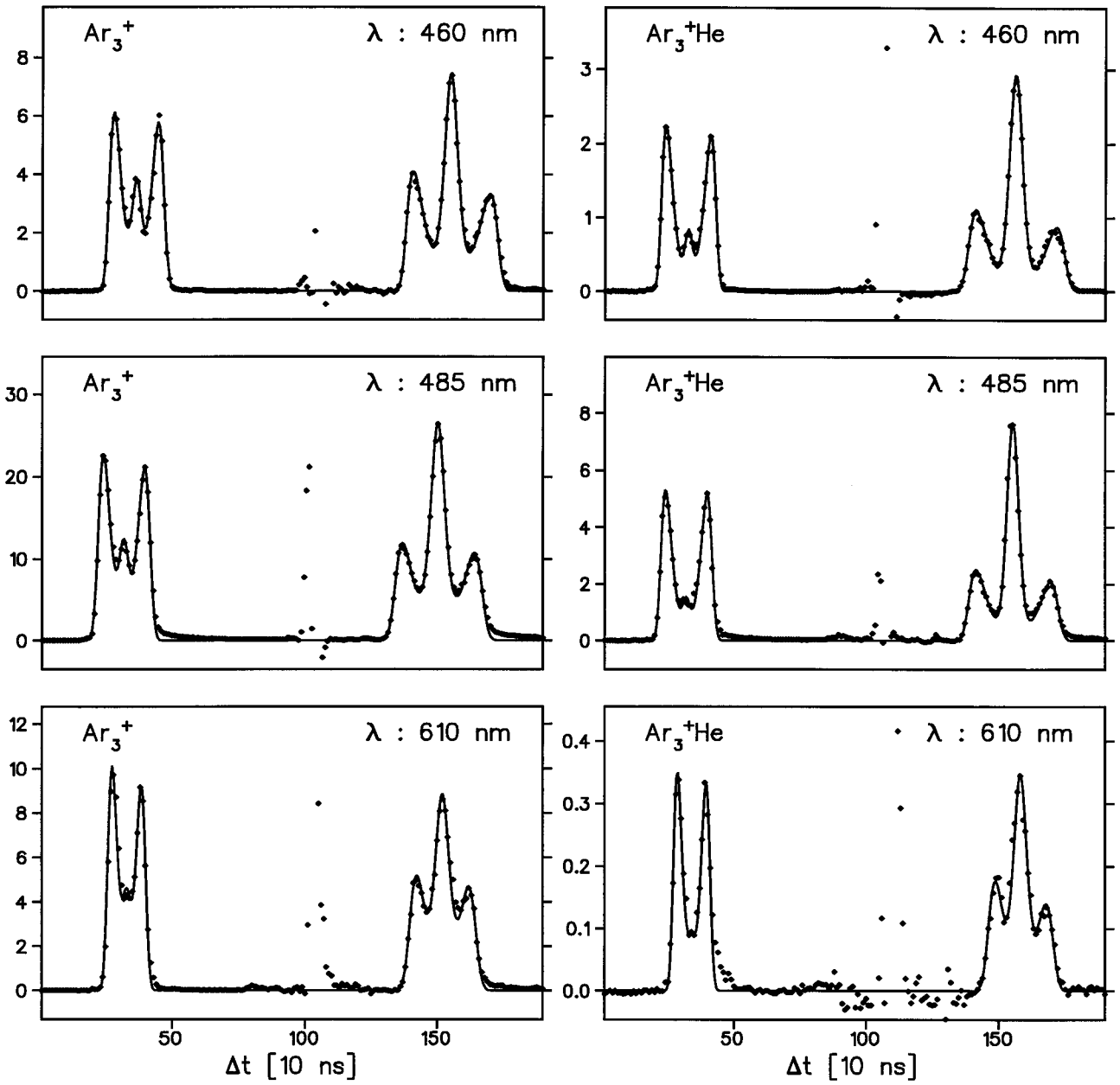

FIG. 8. Fragment TOF spectra of Ar_3^+ and Ar_3^+He at three different wavelengths, laser polarization parallel to the beam. The low internal energy of the argon trimer with the attached helium atom leads to a reduction of the slow Ar_1^+ fragment intensity.

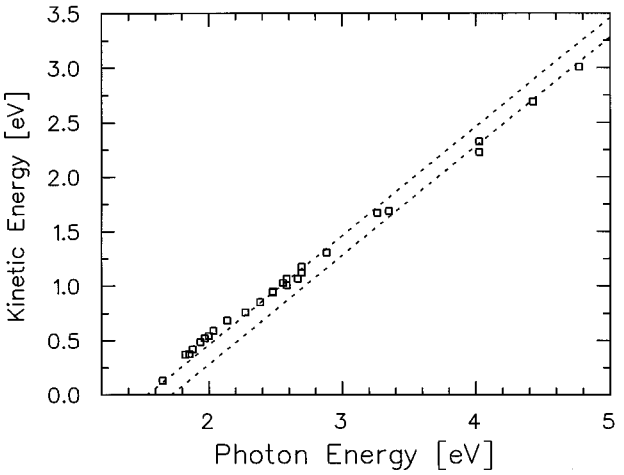

FIG. 9. Total kinetic energy of the photofragments of Ar_3^+ as function of the photon energy. The straight lines indicate the energy calculated from a total binding energy of $D_0=1.54$ eV (Refs. 23 and 24) and neglectable internal energy for the two possible fine-structure states of the ions.

monomers appear. This is not true at wavelengths nearby 400 nm, where a very strong intensity of slow ions appears. Another interesting effect is that in this region the amount of symmetrical fragmentation changes dramatically within a small wavelength range. In Fig. 11, the ratio between symmetrical and asymmetrical dissociation is depicted. Figure 12 finally shows the total kinetic energies of the photofragments. Again the two lines indicate the energies which can be expected for the two fine structure states of the ion, assuming a binding energy of 1.24 eV.[25,26] Near the absorption maxima at 1.75 and 3.1 eV,[11] the measured energies coincidence well with these lines, while at other photon energies a deviation due to vibrational excitation of the trimer can be observed.

V. DISCUSSION

The measured properties of the trimers and especially their fragmentation symmetry will be discussed in this section in terms of their electronic states. The trimers will be treated in the order helium, xenon, and argon, as to follow the increasing complexity of the systems.

A. Helium

The ionized helium trimer is a remarkably easy system. In the energy region of interest, it only has three different electronic states, the molecular orbitals of which together with potential energy curves are schematically shown in Fig. 13. In this simple LCAO description the molecular orbitals only consist of the atomic $1s$ orbitals, which here are symbolized by circles. Five electrons have to be put into these molecular orbitals. In the electronic ground state (Σ_g) all of the orbitals are doubly filled except the antibonding orbital σ_g, which only contains one electron, whereas in the excited Σ_u state the nonbonding orbital σ_u is the half-filled one. As the wave function of the half-filled orbital determines the spatial distribution of the positive charge, there is no charge on the middle atom in this excited state. If this charge distribution is maintained during the fragmentation, only fast ions can be produced, which is exactly what we have observed. A crucial point is the way the wave function can collapse from an equal distribution of the charge on the two outer atoms to the final state where the charge is located only on one of these two. This can be solved by examining the behavior of the charge distribution upon lengthening one of the two bonds of the trimer. As can be shown by a simple Hückel-type LCAO calculation, both the lower and the upper Σ_u state will develop into the Σ_u and the Σ_g state of the charged dimer with no charge residing on the removed atom, while the Σ_g state of the trimer will develop into a neutral dimer and a removed ion. This could explain the localization of the charge; as the excited trimer dissociates, at a sufficiently large distance even a small difference between the two bond lengths will lead to the localization of the charge on the outermost atom. One consequence of this attractively simple model would be that the fast charged fragments should always have a higher velocity than the fast neutral ones, which, however, was not observed in the experiment within the experimental resolution. In any case this charge localization upon asymmetric stretching gives rise to another phenomenon: If one of the bonds is stretched, the optical transition from the former lower Σ_g to the former upper Σ_g state becomes allowed, because with the charge being localized mainly on the two atoms with the shorter distance this transition strongly resembles the $\Sigma_u \rightarrow \Sigma_g$ transition of the charged dimer. For this excited Σ_g state of the trimer the charge localization on slow or fast fragments upon dissociation is not so easy to predict as for the case of the Σ_u state. Symmetry arguments alone give no definite answer, and certainly electron correlation will have an important influence here.

B. Xenon

The ionized xenon trimer is a more complex system. The valence molecular orbitals of this species in a LCAO description consist of the atomic $5p$ orbitals, so that a number of nine orbitals result. Additionally the strong spin–orbit coupling ($\Delta E_{SO}=1.31$ eV) plays an important role. Potential energy curves of the trimer in $D_{\infty h}$ geometry[27] are shown in Fig. 14.

The main optical absorption, which is excited at a wavelength of about 710 nm, is the transition $\Sigma(\frac{1}{2})_u \rightarrow \Sigma(\frac{1}{2})_g$. Like in the case of the helium trimer, in this excited state the charge is located on the outer atoms, and consequently the fragmentation leads to formation of only fast ions. As can be seen in Fig. 10, this is in accordance with experiment. At 400 nm, however, where the transition $\Sigma(\frac{1}{2})_u \rightarrow \Pi(\frac{1}{2})_g$ is excited, which because of the same gerade symmetry should also lead to ejection of only fast ions, a large amount of slow ions are formed as well. Moreover, the ratio of fast to slow ions changes dramatically in a very small wavelength region where no other possible transition should play a role. The reason for this behavior is a curve crossing, or more precisely, a conical intersection between the $\Pi(\frac{1}{2})_g$ and the upper $\Pi(\frac{1}{2})_u$ state at $R \approx 3.6$ Å (Fig. 14). In perfect $D_{\infty h}$ symmetry, these states do not interact due to their different inversion symmetry. Upon bending or asymmetric stretching of the

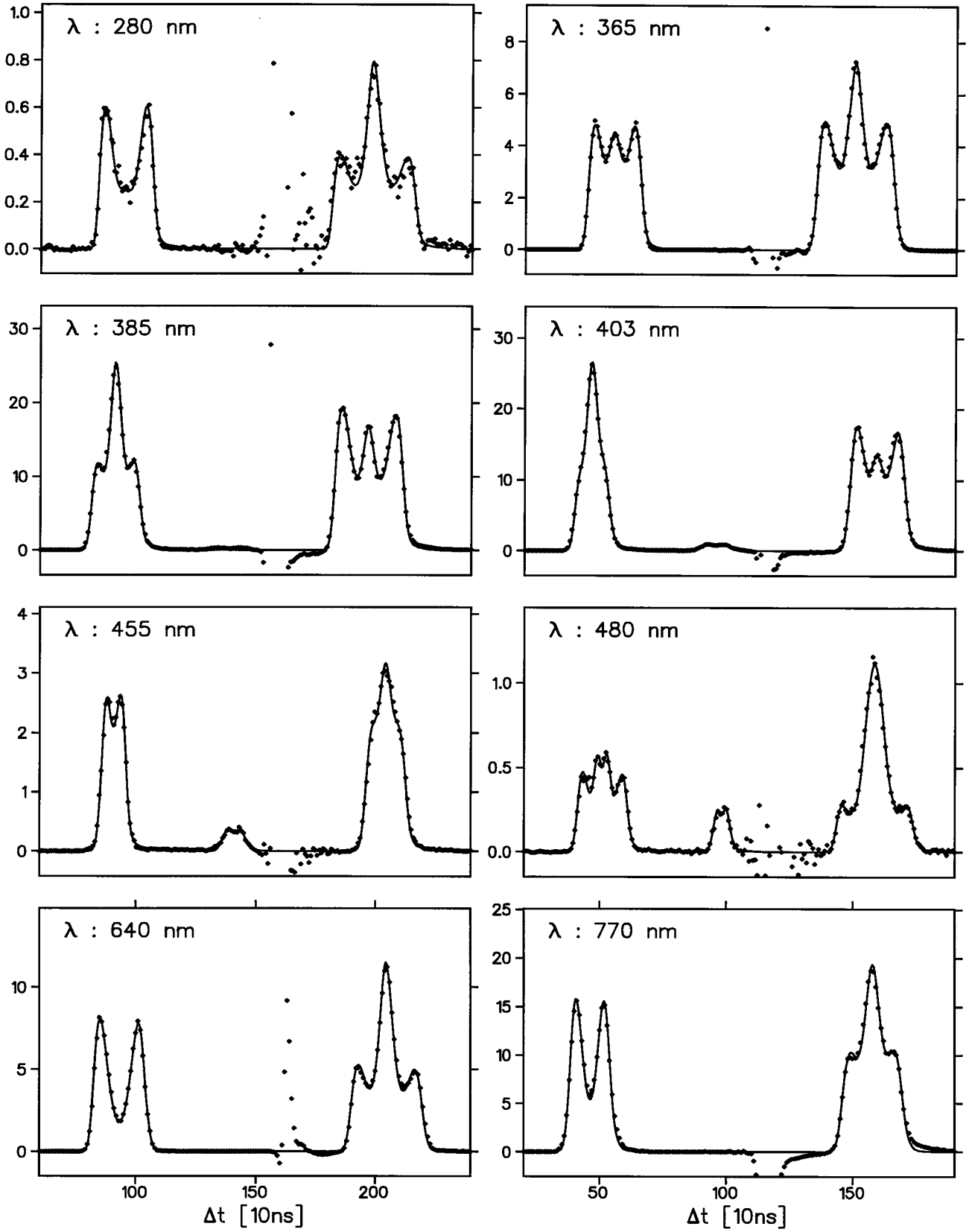

FIG. 10. Fragment TOF spectra of Xe_3^+ at two different wavelengths, laser polarization parallel to the beam. The fragments Xe_1^+ and Xe_1 appear from left to right.

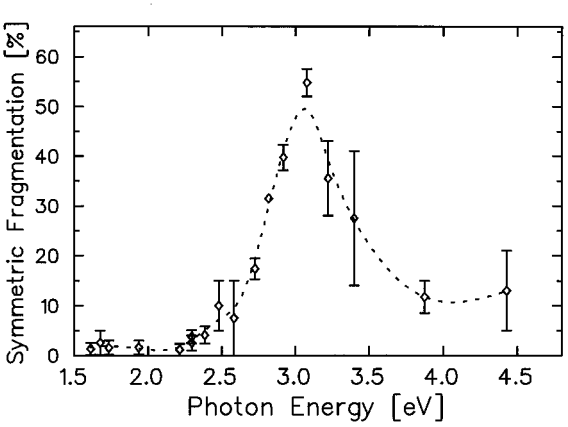

FIG. 11. Amount of symmetric fragmentation of Xe_3^+ as function of the photon energy.

trimer, however, this inversion symmetry has no meaning any more and the states will interact, thus producing an avoided crossing. So if the trimer is excited into the $\Pi(\frac{1}{2})_g$ state and fragments with a slightly distorted symmetry, it will follow the avoided crossing and end up in the former $\Pi(\frac{1}{2})_u$ state, this is with most of the charge localized on the middle, slow atom. The abrupt change of the production of slow ions with wavelength is due to the fact that whether an avoided crossing will be followed or crossed strongly depends on the velocity with which the region of the crossing is passed. So the highest yield of slow ions can be expected for a photon energy at which the trimer is excited into the $\Pi(\frac{1}{2})_g$ state just above the crossing. At lower energies, where the $\Pi(\frac{1}{2})_g$ state is excited below the crossing, no interchange to the ungerade state will take place and only fast ions will appear. This can be seen in Fig. 10. Whereas for 403 nm, a very high intensity of slow ions can be observed, at 455 nm only a pair of wings indicating fast ions is visible.

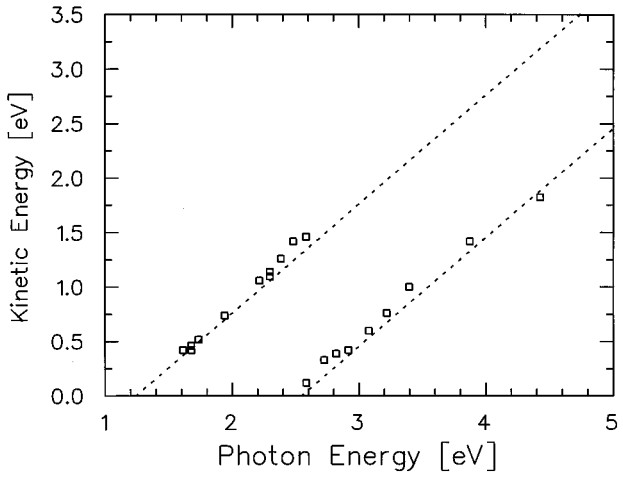

FIG. 12. Total kinetic energy of the photofragments of Xe_3^+ as function of the photon energy. The straight lines indicate the energy calculated from a total binding energy of D_0=1.24 eV (Refs. 25 and 26) and neglectable internal energy for the two possible finestructure states of the ions.

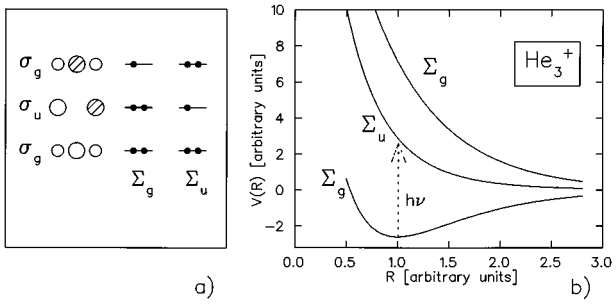

FIG. 13. (a) LCAO description of the three lowest molecular orbitals of He_3^+. (b) Schematic potential energy curves of He_3^+ in $D_{\infty h}$ symmetry.

Rather unexpected is the fragmentation pattern at the highest photon energy of 4.4 eV (280 nm). Although here the transition into the highest $\Sigma(\frac{1}{2})_u$ state should take place, in which about 50% of the charge is located on the middle atom, mainly fast ions are produced. As symmetry considerations do not strictly determine a charge distribution for this case, only calculations can solve this question. Another interesting feature can be seen at about 480 nm. At this wavelength two pairs of wings appear, that is, the fast ions mentioned already and the much faster ions produced by excitation of the $\Sigma(\frac{1}{2})_g$ state. This state asymptotically leads to the lower spin state of the ion, whereby the ions obtain about 1.3 eV of additional kinetic energy.

From the experimental findings obtained so far one can deduce the following hypothesis: excited states of the linear trimers, in which the charge is located only on the outer atoms, will maintain their charge distribution during fragmentation unless they proceed through a curve crossing. This is true for the excited Σ_u state of He_3^+ as well as the excited Σ_g state of Xe_3^+. If, however, in the course of the dissociation a crossing does occur, the change to another state becomes possible, and thus a redistribution of the charge. It should be emphasized that this curve crossings only appear if spin–orbit coupling is taken into account. Nonadiabatic transitions due to vibrational excitations seem to have only a minor

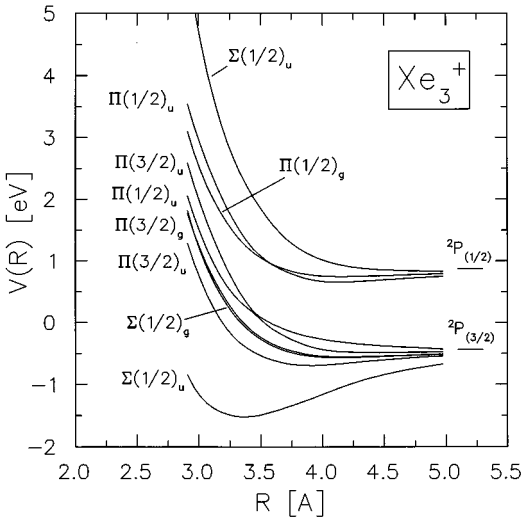

FIG. 14. Potential energy curves of Xe_3^+ in $D_{\infty h}$ symmetry (Ref. 27).

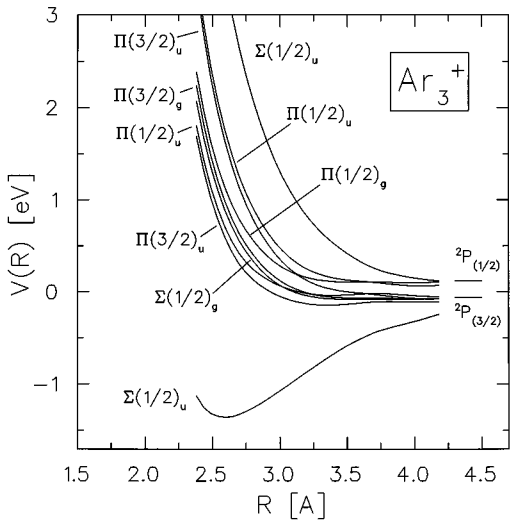

FIG. 15. Potential energy curves of Ar_3^+ in $D_{\infty h}$ symmetry (Ref. 27).

influence, because they do not lead to a significant slow ion intensity in the cases where no curve crossings occurs. Thus numerical simulations of the fragmentation process, which calculate a strong mixing between gerade and ungerade states despite neglect of spin–orbit coupling, obviously overestimate the amount of nonadiabatic transitions.

C. Argon

Inspection of the potential energy curves of the argon trimer (Fig. 15) show that in this system a number of crossings exist in the region of interest. Consequently at many points the transition between gerade and ungerade states is possible, which makes it difficult to predict the development of the charge distribution of certain states upon dissociation. Principally two mechanisms can be responsible for the observed production of slow ions: One is the already described excitation of a gerade state with subsequent transition into an ungerade state, this transition being possible due to vibrational distortion of the trimer symmetry. The second mechanism is the direct excitation of an ungerade state, similarly made possible by asymmetrical vibrational modes. It is not clear how much this second certainly possible process will contribute to the production of the slow ions. As it does not seem to play a role in the photofragmentation of Xe_3^+, it can be assumed that it is also only of minor importance in the case of Ar_3^+. Such a ungerade→ungerade transition may, however, be responsible for the appearance of charged dimer fragments at the low photon energies, since this effect could be due to the excitation of the lower Π_u state, which can dissociate into a bound dimer in the electronic ground state and a neutral atom.[3]

In any case the production of slow charged monomer fragments should depend on the amount of vibrational excitation of the trimer. This is clearly demonstrated by the experiment on the cooled argon trimer. Reduction of the inner energy here obviously leads to a lower abundance of slow ions. This experiment, however, cannot be used to decide which one of the afore described mechanisms for the production of the slow ions is the dominant one. So for the argon trimer the observed production of the slow ions cannot be exactly backtraced. From the comparison with the two other systems it can nevertheless be safely deduced that also here the conical intersections between the potential energy hypersurfaces will have the dominant influence.

VI. SUMMARY

The kinetic energy release to neutral and charged photofragments of He_3^+, Ar_3^+, and Xe_3^+ have been examined in a photon energy range from 1.5 to 6 eV. The measured kinetic energies allow to determine the trimer binding energies and the fine structure state of the charged monomer fragment. In this study the main attention has been put on the wavelength dependence of the symmetry of the charge localization upon dissociation. A comparison of the results obtained for the three different systems indicates that charge redistribution in the course of the dissociation is only to a negligible amount due to nonadiabatic transitions between nearby states of different symmetry. The main mechanism of state interchange instead seems to be the adiabatic passage through avoided crossings, i.e., conical intersections. These conical intersections originate from the bond length dependent state perturbation by spin–orbit coupling and the symmetry disturbance by excitation of asymmetric stretching or bending modes. From these findings it can thus be concluded that the inclusion of spin–orbit coupling is indispensable for calculations of the photodissociation dynamics at least of argon or xenon trimers.

ACKNOWLEDGMENTS

The helium cluster source used in this experiment was made available by the Max Planck Institut für Strömungsforschung, Göttingen. We are indebted to Professor J. P. Toennies for this fruitful cooperation, and to Dr. Ralf Fröchtenicht for organizing the transfer and helping with the installation of the cluster source. We further want to thank Dr. Fernand Spiegelmann for helpful discussions and for kindly providing a DIM computer program. This work has been supported by the Deutsche Forschungsgemeinschaft through SFB 276, TP C5.

[1] W. R. Wadt, Appl. Phys. Lett. **38**, 1030 (1981).
[2] H. U. Böhmer and S. D. Peyerimhoff, Z. Phys. D **4**, 195 (1986).
[3] F. X. Gadea and M. Amarouche, Chem. Phys. **140**, 385 (1990).
[4] Z. Y. Chen, B. D. May, and A. W. Castleman, Z. Phys. D **25**, 239 (1993).
[5] V. Staemmler, Z. Phys. D **22**, 741 (1992).
[6] T. Ikegami, T. Kondow, and S. Iwata, J. Chem. Phys. **99**, 3589 (1993).
[7] F. X. Gadea and J. Durup, Laser Chem. **11**, 95 (1991).
[8] Although the experimental results do not exclude a slight asymmetric distortion of the ground state structure, the state notation of $D_{\infty h}$ symmetry is used throughout this report as it gives the clearest picture of the wave function characters.
[9] N. E. Levinger, D. Ray, M. L. Alexander, and W. C. Lineberger, J. Chem. Phys. **89**, 5654 (1988).
[10] Th. F. Magnera and J. Michl, Chem. Phys. Lett. **192**, 99 (1992).
[11] H. Haberland, B. v. Issendorff, Th. Kolar, H. Kornmeier, Ch. Ludewigt, and A. Risch, Phys. Rev. Lett. **67**, 3290 (1991).
[12] H. Haberland, B. v. Issendorff, R. Fröchtenicht, and J. P. Toennies, J. Chem. Phys. **102**, 8773 (1995).
[13] C. A. Woodward, J. E. Upham, A. J. Stace, and J. N. Murrel, J. Chem. Phys. **91**, 7612 (1989).

[14] C. A. Woodward, B. J. Whitaker, and A. J. Stace, J. Chem. Soc. Faraday Trans. **86**, 2069 (1990).
[15] J. T. Snodgrass, C. M. Roehl, and M. T. Bowers, Chem. Phys. Lett. **159**, 10 (1989).
[16] T. Nagata, J. Hirokawa, T. Ikegami, and T. Kondow, Chem. Phys. Lett. **171**, 433 (1990).
[17] T. Nagata and T. Kondow, J. Chem. Phys. **98**, 290 (1993).
[18] N. G. Gott, R. Hallet, J. A. Smith, and A. J. Stace, Chem. Phys. Lett. **181**, 491 (1991).
[19] H. Haberland, H. Kornmeier, C. Ludewigt, and A. Risch, Rev. Sci. Instrum. **62**, 2621 (1991).
[20] H. Buchenau, J. Northby, E. L. Knuth, J. P. Toennies, and C. Winkler, J. Chem. Phys. **92**, 6875 (1990).
[21] V. Staemmler, Z. Phys. D **16**, 219 (1990).
[22] B. v. Issendorff, Ph.D. thesis, Albert-Ludwigs Universität Freiburg (1994).
[23] J. T. Moseley, R. P. Saxon, B. A. Huber, P. C. Cosby, R. Abouaf, and M. Tadjeddine, J. Chem. Phys. **67**, 1659 (1977).
[24] K. Hiraoka and T. Mori, J. Chem. Phys. **90**, 7143 (1989).
[25] Y. Lu, T. Matsui, K. Tanaka, K. Ito, T. Hayaishi, and Y. Morioka, J. Phys. B **25**, 5101 (1992).
[26] H. Helm, Phys. Rev. A **14**, 680 (1976).
[27] The potential energy curves were calculated with a DIM-program kindly made available by F. Spiegelmann, Universite Paul Sabatier, Toulouse. The program uses dimer potential curves taken from Refs. 28 and 29.
[28] M. Daskalopoulou, H.-U. Böhmer, and S. D. Peyerimhoff, Z. Phys. D **15**, 161 (1990).
[29] W. J. Stevens, M. Gardner, A. Karo, and P. Julienne, J. Chem. Phys. **67**, 2860 (1977).